# Lifetime measurements in $^{180}$Pt

Q. M. Chen,[1] X. G. Wu,[1,*] Y. S. Chen,[1] C. B. Li,[1] Z. C. Gao,[1,†] G. S. Li,[1] F. Q. Chen,[1] C. Y. He,[1] Y. Zheng,[1] S. P. Hu,[1] J. Zhong,[1,2] Y. H. Wu,[1,3] H. W. Li,[1,3] and P. W. Luo[1,2]

[1]*China Institute of Atomic Energy, Beijing 102413, China*

[2]*College of Physics and Technology, Shenzhen University, Shenzhen 518060, China*

[3]*College of Physics, Jilin University, Changchun 130012, China*

(Received 18 August 2015; revised manuscript received 11 March 2016; published 12 April 2016)

Lifetimes of the yrast states in $^{180}$Pt have been measured from $4^+$ to $8^+$ using the recoil distance Doppler-shift technique in the coincidence mode. These states were populated by the reaction $^{156}$Gd($^{28}$Si ,$4n$)$^{180}$Pt at a beam energy of 144 MeV. The differential decay curve method was applied to determine the lifetimes from experimental coincidence data. The $B(E2)$ values extracted from lifetimes increase with increasing spin, implying rotor behavior, but do not show the typical shape coexistence where the $B(E2)$ values present a rapid increase at very low spins. Calculations based on the triaxial projected shell model were performed for the yrast states in $^{180}$Pt and the results of both energies and $E2$ transition probabilities reproduce the experimental data very well. The result also shows that a better description of the yrast band in $^{180}$Pt requires consideration of the $\gamma$ degree of freedom.

DOI: 10.1103/PhysRevC.93.044310

## I. INTRODUCTION

Shape coexistence has been observed in many nuclei with protons or neutrons at and near closed shells [1–3]. This phenomenon becomes more apparent in the $A = 180$ region where the proton number is equal or close to 82 and the neutron Fermi level is around midshell, for example, in the Hg ($Z = 80$) and Pb ($Z = 82$) isotopes [4–6]. The observed two low-lying excited $0^+$ states and the ground states in $^{186,188}$Pb are interpreted to be the prolate, oblate, and spherical states, respectively. In $^{182,184,186,188}$Hg, the low-lying excited $0_2{}^+$ states and the ground states are suggested to be prolate and oblate, respectively. It appears that low-lying excited $0^+$ states are associated with shape coexistence. In contrast, the shape-coexistence picture in Pt ($Z = 78$) nuclei has been a matter of argument and engendered extensive interest in recent years [7–12]. The low-lying $0_2{}^+$ excited states in even-even Pt isotopes from $^{178}$Pt to $^{186}$Pt have been observed at around 500 keV above the ground state, and this also has been suggested as evidence of shape coexistence. And the level spacings in the $0_2{}^+$ bands observed in these even-even Pt isotopes differ from the rotational band which characterizes a deformed rotor. However, the potential energy surfaces (PES) calculated for the even Pt isotopes have no second local minimum that is proposed by the shape-coexistence picture [13–17], and this indicates that the PES calculations do not support the interpretation of the low-lying $0_2{}^+$ state as having a distinctly different quadrupole deformation than for the ground state. The minima in the energy surface are of pure mean-field configurations, while configuration mixing could not be taken into account. The level spacings observed in the yrast bands of these Pt isotopes present dramatic changes with neutron numbers, characterizing the transitional Pt region where the strong nuclear configuration mixing that plays an important role in the structure of very light Pt nuclei.

In addition to the appearance of the low-lying $0_2{}^+$ states, the rapid increase of the $E2$ transition probabilities, $B(E2)$ values, of the yrast states with increasing spin at very low spins provides another signature for the shape coexistence [1,18]. Further studies of the complex structures in these transitional Pt nuclei require the systematics of experimental $E2$ transition probability. The $E2$ transition probabilities contain the essential information on nuclear deformations, and the lifetime measurement is a direct way to determine the absolute $B(E2)$ values. The experimental systematics of the quadrupole deformation extracted from the corresponding $B(E2)$ values has a deep impact on the understanding of nuclear structure and its evolution in functions of both neutron number and spin. For the nucleus $^{180}$Pt, no previous lifetime values were published on the excited states above $4_1{}^+$ although its plentiful levels have been measured very well [19].

In this paper, we present the lifetime measurements for states of the yrast band in $^{180}$Pt based on the use of the recoil distance Doppler-shift (RDDS) technique. Sections II and III describe the experiment, data analysis, and results. In Sec. IV the systemtics of experimental $B(E2)$ values in Pt isotopes are discussed and theoretical calculations also performed based on the triaxial projected shell model. The conclusions are summarized in Sec. V.

## II. EXPERIMENT

### A. The plunger apparatus

The RDDS technique, also called recoil distance method (RDM), is the standard method for measuring lifetimes of excited nuclear states in the picosecond range. Because of the Doppler effect, the energies of the $\gamma$ rays emitted by the stopped and moving nuclei are different. The lifetimes of excited states in the recoiling nuclei can be then determined directly from the ratio of shifted and unshifted intensities of decaying transitions. More detailed information of this technique can be found in the review article [20] and references therein. The core apparatus of this technique is the plunger

*Corresponding author: wxg@ciae.ac.cn

†Corresponding author: zcgao@ciae.ac.cn

 ©2016 American Physical Society

that mounts target- and stopper-foil and is housed in a target chamber. The design of the China Institute of Atomic Energy (CIAE) plunger, built at our laboratory in 2012, is similar to the Cologne plunger [21] as well as the New Yale plunger device (NYPD) [22]. There are three main parts of the CIAE plunger, including base plate, sliding stage, and support frames. Two support frames mount the target and stopper foils, respectively, and make them perpendicular to the beam direction. The stopper frame is fixed in the center of the target chamber, whereas the target frame is situated on the sliding stage, which ensures precise linear motion of the target in beam direction. The sliding stage is an N-661 miniature linear stage driven by an E-861 controller. Both the N-661 and the E-861 were purchased from the Physik Instrumente (PI) corporation of Germany. The N-661 stage integrates a piezo stepping linear motor combined with a high-resolution linear encoder. It provides 18 mm travel and a resolution down to the nanometer rang [23]. In practice, the space resolution of the N-661 stage is 0.3 $\mu$m checked by means of laser interferometry. In order to reach very small target-to-stopper separations, the surface of foils have to be very clean and stretched. The target and stopper foil are first glued on aluminium rings and then stretched by screwing these rings on support rings with conical shapes in the center. These cones, having the central hole with a diameter of 8 mm, determine the plane of the target and the stopper. The cones are well polished where the foils touch them. The target and stopper foils are adjusted parallel to each other and electrically insulated from the aluminium base plate and the target chamber.

Target-to-stopper distances can be directly given by the N-661 stage with high resolution. These distance values are obtained with the cold apparatus. During the in-beam experiment, however, the stability of target-to-stopper distances would be disturbed by mechanical vibrations and by deformations of the foils caused by thermal expansion from beam bombardment. Therefore, it is necessary to compensate the resulting changes of the distance by a feedback mechanism. The design of our feedback system was based on the high-resolution linear encoder in the N-661 miniature linear stage. Using this encoder, a control program was developed to drive the motor in the N-661 stage with the resolution of 0.3 $\mu$m. In practice, the feedback system permanently monitors the changes of target-to-stopper distance by measuring the capacitance of the two foils and makes correction of the distance in time by driving the motor in N-661 stage. In this feedback system, capacity calibration, or comparatively distance calibration, has been performed. The calibration data can be used as a standard database for the correction of target-to-stopper distance in the feedback system. The capacitance is measured by the TH2817A Precision LCR Meter purchased from the Changzhou Tonghui corporation and the capacitance resolution is 0.00001 pF [24], which can distinguish a separation rather smaller than 0.1 $\mu$m. The meter continuously provides a measuring signal with the frequency of 100 kHz. This frequency would be modified due to the effect of target-to-stopper capacitance, and, in turn, by analyzing the modified frequency the capacitance can be determined. The meter also provides an inner trigger with the rate of 30 events per second. Thus, for every 1/30 second a capacitance measurement is performed, and the corresponding distance is then obtained. Once the deviation between this distance and the one in calibration database exceeds 0.3 $\mu$m, the N-661 stage is moved to compensate the distance change. The high-performance range of the feedback system is 0–200 $\mu$m. When the separation exceeds the upper limit of the range, the feedback precision will be relaxed, but at this time the N-661 miniature linear stage can still guarantee a high enough relative resolution itself.

### B. Experimental procedure

Excited states in the nucleus $^{180}$Pt were populated via the reaction $^{156}$Gd($^{28}$Si ,4n)$^{180}$Pt at a beam energy of 144 MeV provided by the HI-13 tandem accelerator at China Institute of Atomic Energy (CIAE). The target was isotopically enriched $^{156}$Gd evaporated to a thickness of 500 $\mu$g/cm$^2$ onto a stretched 2.0 mg/cm$^2$ thick gold foil serving as a backing and facing the beam. After a flight in vacuum with a mean velocity of 1.32% of light velocity $c$, the recoiling nuclei were stopped in a 4.0 mg/cm$^2$ gold foil. Both of the Gd/Au and Au foils were mounted in the CIAE plunger apparatus. The distances were set by moving the target holder. Coincident de-exciting $\gamma$ rays were recorded with an array consisting of 9 Compton-suppressed HPGe detectors and 2 planar HPGe detectors. Two of the Compton-suppressed HPGe detectors were situated at angle 42°, three at 90°, and four at approximately 153° with respect to the beam direction, respectively. In the measurement, $\gamma\gamma$-coincidence data were taken at 12 target-to-stopper distances ranging from 2 to 450 $\mu$m, and for each distance it took approximately 4 h. In addition, the distance of 0 $\mu$m was taken at the electrical contact between the target and stopper foils. A total of 23.2 $\times$ 10$^6$ doubles and higher-fold events were collected. As part of the experiment, energy and efficiency calibrations for detectors were made with $^{152}$Eu and $^{133}$Ba sources. The mean recoil velocity of the nuclei $^{180}$Pt was deduced from the energy difference in the shifted and unshifted peaks for the yrast transitions of the $4_1^+$, $6_1^+$, $8_1^+$, and $10_1^+$ levels.

## III. DATA ANALYSIS AND RESULTS

### A. The differential decay curve method (DDCM)

For the analysis of coincidence RDDS data, the differential decay curve method (DDCM) developed in Refs. [20,25,26] is an optimal alternative. From the coincidence data, the gated-above spectra can be generated by gating on Doppler-shifted components of feeding transitions lying higher in the cascade above the levels of interest. Based on these gated-above spectra, the lifetimes of the levels of interest can be then determined. A crucial aspect of the data analysis for RDDS data was accounting for the effects of level feeding, both observed and unobserved, from higher-lying states. By means of the gating procedure, the feeding patterns are considerably simplified and problems related to unobserved feeders can be eliminated. However, the performance of the gating procedure requires a large number of $\gamma$-ray counts collected for achieving good statistics. In the present work, with a few tens of million doubles and higher-fold events collected, the obtained

lifetimes of the yrast states up to $8^+$ are able to provide statistical confidence.

Here, we briefly describe the main points of the DDCM. If a level of interest is directly populated by transition B and depopulated by transition A, the lifetime $\tau(x)$ of the level is determined at each target-to-stopper distance $x$ by the expression [20,26]

$$\tau(x) = \frac{\{B_s, A_u\}(x)}{\frac{d}{dx}\{B_s, A_s\}(x)} \frac{1}{\langle v \rangle}, \quad (1)$$

where $\langle v \rangle$ is the mean velocity of the recoiling nuclei and $\{B_s, A_{s(u)}\}(x)$ is the shifted (unshifted) intensity for transition A in coincidence with the shifted component of transition B at distance $x$.

According to Eq. (1), only the coincidence intensities of transition A are used to determine the values of $\tau$. Also only relative target-to-stopper distances are required. The lifetime values are then independent of the distance at which they have been determined and correspondingly should be constant when plotted versus distance. In addition, by gating only on the shifted component of a direct feeding transition, the effect of nuclear deorientation cancels out completely and does not influence the results of the lifetime analysis [27].

In determining lifetimes, the intensities of the shifted and unshifted components of transitions have to be corrected for differences in running time and beam intensity for different distances and normalized to the total number of reactions per distance. In the present work, the normalization was done by choosing a normalization factor such that the intensity of the 279-keV transition due to the Coulomb excitation of $^{197}$Au, collected by detectors placed at 90°, remains constant for all the distances.

In order to improve the gated-above spectra, three matrices (backward-backward, forward-forward, and backward-forward) were built at each distance. First is the symmetric matrix that covers spectra measured with four detectors positioned at 153°. Second is the symmetric matrix that covers spectra measured with two detectors positioned at 42°. Third is an asymmetric matrix covering spectra measured with four detectors positioned at 153° and two at 42°. For a given level, gates on the shifted component of the direct feeding transition were set in the $\gamma$-$\gamma$ matrices and the four gated-above spectra are then obtained at each distance. The four spectra can be summed up into two resulting spectra, namely, backward angle spectrum (coincidence data taken with the detectors at 153°) and forward angle spectrum (coincidence data taken with the detectors at 42°). The lifetimes determined from the two resulting spectra are statistically independent and, hence, allow a consistency check. The final value of the lifetime for the level of interest was derived by averaging the individual results. The possible contaminants in the energy of the peaks of interest were also checked by using the spectra measured with the three detectors positioned at 90°.

Figure 1 shows part of the backward angle spectra of the transitions of $4_1^+ \rightarrow 2_1^+$, $6_1^+ \rightarrow 4_1^+$, and $8_1^+ \rightarrow 6_1^+$ of $^{180}$Pt obtained with a gate set on the shifted component of the transitions of $6_1^+ \rightarrow 4_1^+$, $8_1^+ \rightarrow 6_1^+$, and $10_1^+ \rightarrow 8_1^+$, respectively. The depopulating transitions of levels of $4_1^+$, $6_1^+$, and $8_1^+$ were measured at each indicated distance with four detectors at 153° in coincidence with the shifted component of the direct feeding transitions measured with six detectors at non-90°. The changes in the relative intensities of the Doppler-shifted and unshifted components of these depopulating transitions with respect to the change in target-to-stopper distances are visible.

Figure 2 illustrates the lifetime analysis for the $4_1^+$ level in $^{180}$Pt using backward angle spectra. The shifted intensities $I_s$ of the $4_1^+ \rightarrow 2_1^+$ transition, measured with the detectors positioned at 153° in coincidence with the shifted component of the $6_1^+ \rightarrow 4_1^+$ transition measured with six detectors positioned at non-90°, are presented in Fig. 2(b), together with the curve corresponding to a piecewise fit with second-order polynomials. According to Eq. (1), the unshifted intensities $I_u$ of the $4_1^+ \rightarrow 2_1^+$ transition measured at the same gating conditions divided by the derivative of the fitted $I_s$ polynomials yield the values of lifetime for each distance, and the resulting lifetime was then obtained by averaging the individual results. The mean lifetime value for the $4_1^+$ level and its uncertainties are shown in Fig. 2(a). For a self-consistency check, the quantity made by multiplying the derivative of the shifted intensity $I_s$ and the lifetime, displayed as a curve, is compared with the unshifted intensities $I_u$ of the $4_1^+ \rightarrow 2_1^+$ transition, and a good agreement between them was achieved, as shown in Fig. 2(c). As a result, the obtained lifetime value for the $4_1^+$ level in $^{180}$Pt is $54.1 \pm 6.6$ ps, marked in the upper right corner of Fig. 2(a). Figures 3 and 4 are the lifetime analyses as in Fig. 2, but for $6^+$ and $8^+$ levels, respectively. The decaying transitions from the levels are in coincidence with the shifted component of the direct feeding transitions of $8_1^+ \rightarrow 6_1^+$ and $10_1^+ \rightarrow 8_1^+$, respectively.

In the derivation of the mean value of lifetime, not all individual lifetime data are used but only those which lie within the so-called region of sensitivity. In the present work, this sensitive region covers the interval of distances where the error bar for the individual lifetime is not too large and the quantities $\{B_s, A_s\}(x)$ and $\{B_s, A_u\}(x)$, participating in the right-hand side of Eq. (1), are not too small, similar to those in Ref. [28]. When carrying out the polynomial fit, we have followed previous experiences where a few data points at small and large distances are not included empirically. In Figs. 3 and 4, the first distance point was abandoned based on the consideration that including this point into the polynomial fit would lead to a bad self-consistency check; namely, the agreement between $I_u$ and $\tau \cdot dI_s/dx$ could be poor. The last two points are not included because they are out of the sensitive range of the distance (the error bars of these two lifetimes are very large).

Figure 5 illustrates the lifetime analysis for the $4_1^+$ level as in Fig. 2, but using forward angle spectra. The resulting value of the lifetime is almost equal to the one obtained in Fig. 2 where the backward angle spectra are used. The final value of the lifetime of the $4_1^+$ level was then obtained by averaging these two results. Due to weaker statistics, the lifetimes of the $6_1^+$ and $8_1^+$ levels cannot be derived reliably using forward angle spectra and the lifetime values for these two levels have been determined only by using backward angle spectra. A summary of the lifetimes of the three states is given in the third column of Table I.

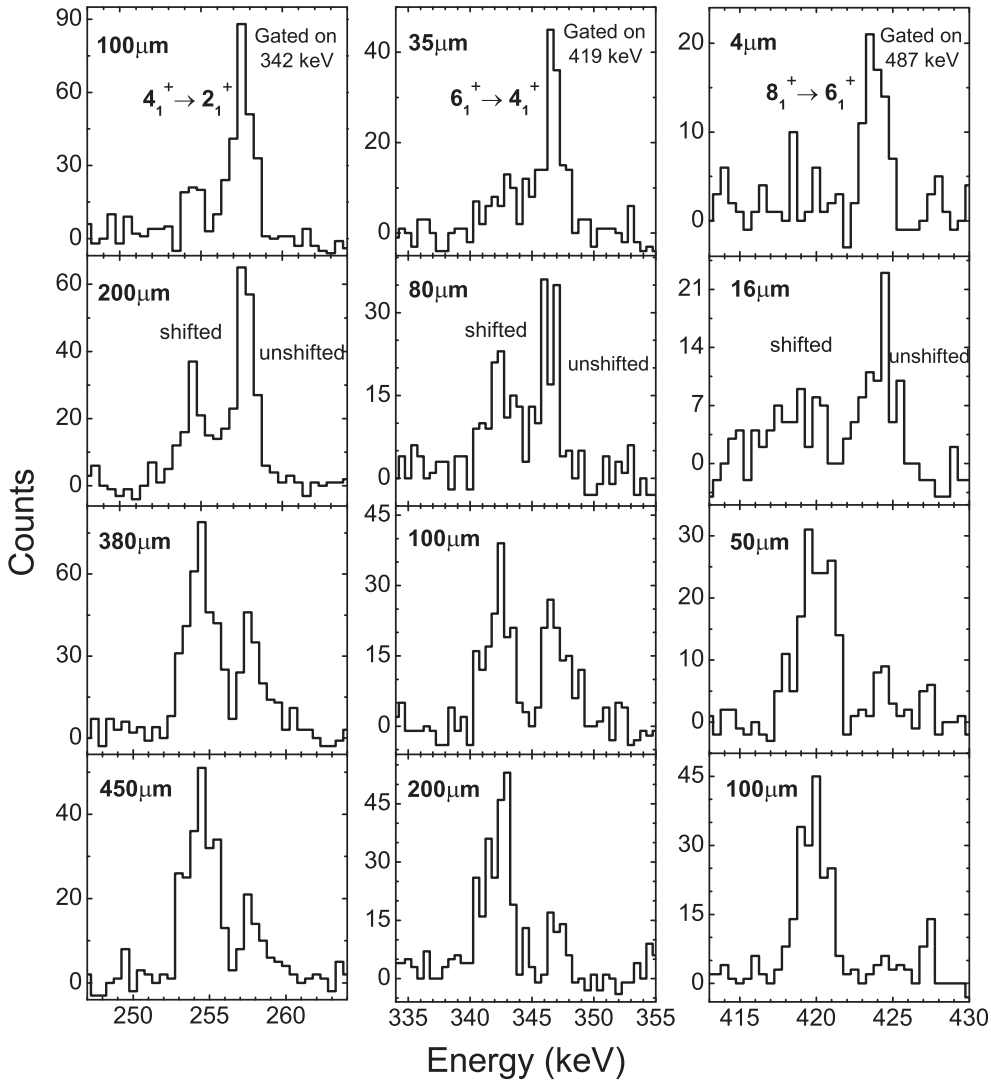


FIG. 1. Spectra of the transitions of $4_1^+ \rightarrow 2_1^+$, $6_1^+ \rightarrow 4_1^+$, and $8_1^+ \rightarrow 6_1^+$ of $^{180}$Pt obtained with a gate set on the shifted component of the transitions of $6_1^+ \rightarrow 4_1^+$, $8_1^+ \rightarrow 6_1^+$, and $10_1^+ \rightarrow 8_1^+$, respectively. These depopulating transitions of levels of $4_1^+$, $6_1^+$, and $8_1^+$ were measured at each indicated distance with four detectors positioned at 153°, in coincidence with the shifted component of the direct feeding transitions measured at the corresponding distance with four detectors positioned at 153° and two at 42°.

The values of the reduced $E2$ transition probabilities can be extracted from lifetimes by the expressions [29]

$$B(E2)_{(e^2b^2)} = \frac{0.0816 R_b}{\tau E_\gamma^5 (1+\alpha)}, \tag{2}$$

$$B(E2)_{(\mathrm{W.u.})} = 1.6834 \times 10^5 A^{-4/3} B(E2)_{(e^2b^2)}, \tag{3}$$

where $\tau$ is the lifetime of the level of interest in picosecond units, $E_\gamma$ is the transition energy in MeV units, $R_b$ is the branching ratio, and $\alpha$ is the conversion coefficient. In the calculation of $B(E2)$ values, $R_b = 1$, the values of $E_\gamma$ are taken from Ref. [19] and the value of $\alpha$ is from nuclear data sheets [30]. The reduced transition probabilities $B(E2)$ are shown in columns 4 and 5 of Table I in $e^2$b$^2$ and Weisskopf (W.u.) units, respectively. Column 6 of Table I presents the corresponding transition quadrupole moments, $Q_t$, obtained from the reduced $E2$ transition probabilities by using the relationship

$$B(E2, I \rightarrow I-2) = \frac{5}{16\pi} \langle I020 | I-20 \rangle^2 Q_t^2. \tag{4}$$

## IV. DISCUSSION

### A. $B(E2)$ experimental systemtics

Three lifetimes of the yrast states from $4_1^+$ to $8_1^+$ for $^{180}$Pt have been determined in the present work. The resulting lifetimes and the corresponding $B(E2)$ values are summarized in Table I.

The lifetime of the $4_1^+$ state in the present work is $53.3 \pm 4.5$ ps, which is much different compared to previously reported values of $75 \pm 15$ ps [19] and $33 \pm 4$ ps [31], which differ from each other by more than a factor of 2. The corresponding $B(E2; 4_1^+ \rightarrow 2_1^+)$ value is $1.16 \pm 0.10$ $e^2b^2$ ($193.1 \pm 16.3$ W.u.), which also significantly differs from

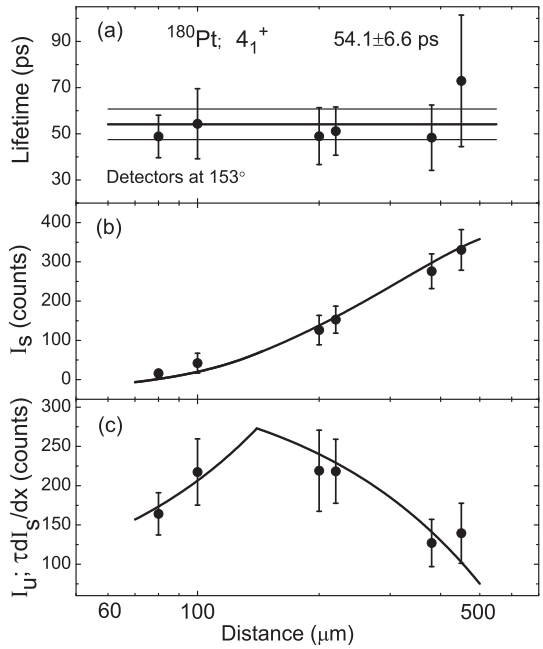


FIG. 2. Lifetime analysis for the $4_1^+$ level in $^{180}$Pt using backward angle spectra. (a) The determined lifetimes, and the mean value and its uncertainties. (b) The shifted intensities $I_s$ of the $4_1^+ \rightarrow 2_1^+$ transition, measured in coincidence with the shifted component of the feeding transition of $6_1^+ \rightarrow 4_1^+$, and the curve corresponding to a piecewise fit with second-order polynomials. (c) The production of the lifetime and the derivative of the shifted intensity $I_s$, compared with the unshifted intensities $I_u$ of the $4_1^+ \rightarrow 2_1^+$ transition for a self-consistency check.

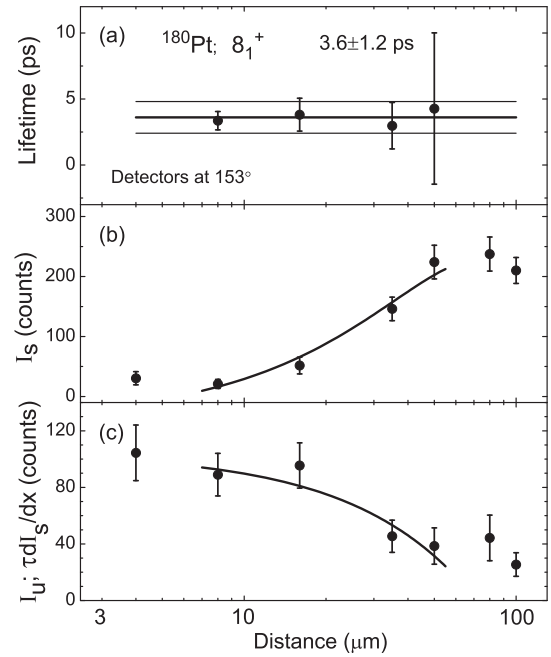


FIG. 4. Lifetime analysis as in Fig. 2, but for the $8_1^+$ level.

the previous values of $0.85 \pm 0.18\ e^2b^2$ ($140 \pm 30$ W.u.) and $1.57 \pm 0.19\ e^2b^2$ ($260 \pm 32$ W.u.). These lifetimes for the same state were measured independently by different experimental groups but using the same RDDS technique. To evaluate the lifetimes of the $4_1^+$ level for $^{180}$Pt, we have illustrated in Fig. 6 the reduced $E2$ transition probabilities $B(E2; 2_1^+ \rightarrow 0_1^+)$ and $B(E2; 4_1^+ \rightarrow 2_1^+)$, and also the $B_{4/2}$ value, defined as $B(E2; 4_1^+ \rightarrow 2_1^+)/B(E2; 2_1^+ \rightarrow 0_1^+)$, for even-even Pt isotopes with $98 \leqslant N \leqslant 108$. As shown in Fig. 6(a), the value of $B(E2; 4_1^+ \rightarrow 2_1^+)$ for $^{180}$Pt, determined in the present work, matches well with the corresponding $B(E2)$ systematics of Pt. We also note that the value $B(E2; 2_1^+ \rightarrow 0_1^+)$, reported by Voigh *et al.* [19], matches well with the corresponding

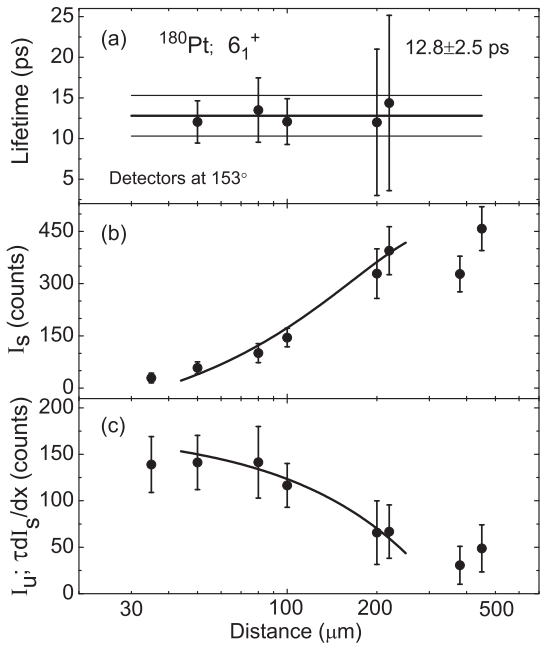


FIG. 3. Lifetime analysis as in Fig. 2, but for the $6_1^+$ level.

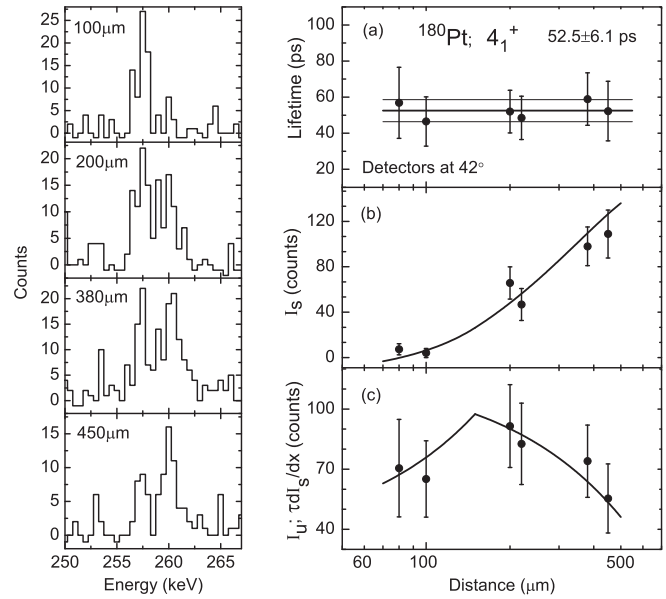


FIG. 5. Lifetime analysis for the $4_1^+$ level; the left and right panels are as same as in Figs. 1 and 2, respectively, but using the forward angle spectra.

TABLE I. Lifetimes, corresponding $B(E2)$ values, and transition quadrupole moments $Q_t$ for the yrast band of $^{180}$Pt.

| $E_\gamma$ [keV] | $I_i \to I_f$ | $\tau$ [ps] | $B(E2)$ [$e^2b^2$] | $B(E2)$ [W.u.] | $Q_t$ [$eb$] |
|---|---|---|---|---|---|
| 257.6 | $4^+ \to 2^+$ | $53.3 \pm 4.5$ | $1.16 \pm 0.10$ | $193.1 \pm 16.3$ | $6.41 \pm 0.27$ |
| 346.5 | $6^+ \to 4^+$ | $12.8 \pm 2.5$ | $1.20 \pm 0.23$ | $198.4 \pm 38.7$ | $6.19 \pm 0.60$ |
| 424.3 | $8^+ \to 6^+$ | $3.6 \pm 1.2$ | $1.59 \pm 0.53$ | $263.1 \pm 87.7$ | $6.97 \pm 1.16$ |

$B(E2)$ systematics of Pt. The two previous $B(E2; 4_1^+ \to 2_1^+)$ values were also presented in Fig. 6(a), and both values show bad systematics, lying too low or too high, respectively. Compared to the two previous $B_{4/2}$ values of $0.9 \pm 0.2$ [19] and $1.7 \pm 0.3$ [31], the present $B_{4/2}$ value of $1.26 \pm 0.16$ matches better with the $B_{4/2}$ systematics of Pt, as shown in Fig. 6(b).

In addition, using the lifetime of $33 \pm 4$ ps for the $4_1^+$ state, reported by Williams *et al.* [31], we obtain $B(E2; 4_1^+ \to 2_1^+) = 312 \pm 38$ W.u. and $B_{4/2} = 2.0 \pm 0.4$, which are larger than their reported values. This means both the $B(E2; 4_1^+ \to 2_1^+)$ value and the $B_{4/2}$ ratio in $^{180}$Pt would present a more sudden change apart from the neighbor Pt isotopes, and this indicates that the lifetime of $4_1^+$ state measured in the present work should be more reasonable.

As an empirical role, the size of $B_{4/2}$ ratio may characterize the nature of the yrast band, a pure geometric vibrator has $B_{4/2} = 2$ [37], while an ideal rotor is manifested by a $B_{4/2}$ of 1.43 [38]. The present $B_{4/2}$ ratio is $1.26 \pm 0.16$, which implies the collective rotor nature of the yrast band for $^{180}$Pt, like a rotor. The $B_{4/2}$ for $^{178}$Pt is $1.36 \pm 0.15$, indicating the rotor nature of the yrast band as well. For other neighbor Pt isotopes, $^{176,182,184,186}$Pt, the $B_{4/2}$ values are around 1.6, as shown in Table II, indicating their soft rotor nature. The $B(E2)$ values may also empirically provide information on the shape coexistence that has been argued for the platinum isotopes. In the case of the shape coexistence, the $B(E2)$ value of the yrast band increases rapidly with increasing spin at low spins, more precisely before back-bending. Compared to the neighboring even nuclei $^{182,184}$Pt, the $B(E2)$ values of the yrast band for $^{180}$Pt present no rapid increase with increasing spin, indicating its shape coexistence is not apparent.

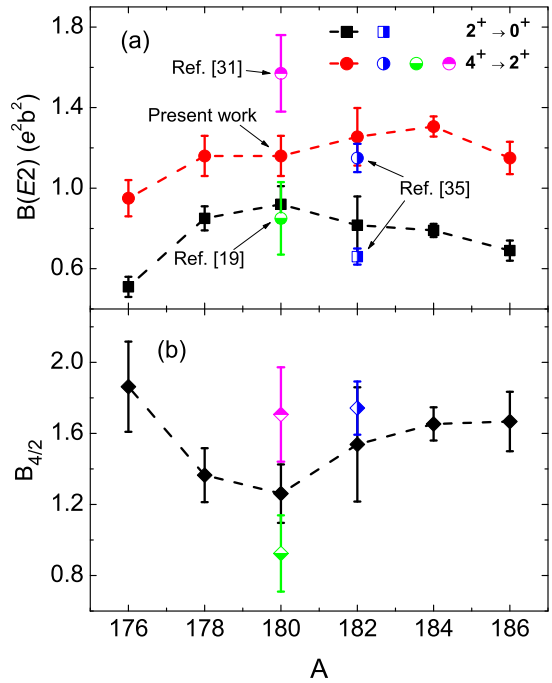


FIG. 6. Experimental (a) $B(E2; 4_1^+ \to 2_1^+)$ and $B(E2; 2_1^+ \to 0_1^+)$ values, and (b) $B_{4/2}$ values for even Pt isotopes with $98 \leqslant N \leqslant 108$. The $B(E2; 4_1^+ \to 2_1^+)$ and the $B_{4/2}$ values for $^{180}$Pt measured in present work are compared with two previous experimental data taken from Ref. [19] (shown in green) and Ref. [31] (shown in magenta). The $B(E2)$ values for $^{176}$Pt and $^{178}$Pt are taken from Refs. [32,33]. There are two sets of experimental transition data for $^{182}$Pt, one from Ref. [34] (shown in black square and red circle) and an other from Ref. [35] (shown in blue). The $B(E2)$ values for $^{184}$Pt are taken from Ref. [36] and that for $^{186}$Pt from Ref. [35].

The experimental evidence for the shape coexistence may be provided by the appearance of the very low-lying second $0^+$ state in the even-even nuclei. The excitation energy of the $0_2^+$ states for $^{176-186}$Pt are about 500 keV above the corresponding ground states [12]. These $0_2^+$ states cannot be regarded as quasiparticle excitations because of such low excitation energy, but may be considered to be of different deformation origin in contrast to the ground states. In $^{180,182,184}$Pt, the $R_{4/2}$ ratios, defined as $E(4^+)/E(2^+)$, are around 2.7 for yrast bands and only about 2.1 for the $0_2^+$ bands, as shown in Table II. This implies that the yrast bands and the $0_2^+$ bands have different momentums of inertia and, therefore, different deformations. However, the sudden change of the behavior of the experimental $B(E2)$ value, presented when going from $^{180}$Pt to $^{182}$Pt, may imply a change in the shape coexistence structure, although the $0_2^+$ band has similarly low excitation energy for these two nuclei. To investigate the possible structure change, the triaxial projected shell model calculations of the yrast bands for $^{178,180,182,184}$Pt have been performed.

### B. The TPSM calculation

The triaxial projected shell model (TPSM) has been applied successfully to describe the moments of inertia in transitional nuclei [40] and the high-spin states in triaxial nuclei [41]. TPSM follows the basic philosophy of the standard shell model and the only difference is that the TPSM starts with the deformed basis to achieve a sufficient truncation for the model space so that the deformed and heavy nuclei can be described within the framework of shell model; see Ref. [41] for details.

The TPSM wave function can be written as

$$|\Psi^\sigma_{IM}\rangle = \sum_{K\kappa} f^\sigma_{IK\kappa}\, \hat{P}^I_{MK} |\Phi_\kappa\rangle, \tag{5}$$

TABLE II. $R_{4/2}$ values observed for the yrast band and the $0_2^+$ band in even $^{176-186}$Pt, as well as $B_{4/2}$ values for the yrast band. The $B_{4/2}$ values for $^{180}$Pt is obtained in the present work, and other $B(E2)$ values are taken from the same references as in Fig. 6 and their energies are from nuclear data sheets [30,39].

| | $^{176}$Pt | $^{178}$Pt | $^{180}$Pt | $^{182}$Pt | $^{184}$Pt | $^{186}$Pt |
|---|---|---|---|---|---|---|
| $B_{4/2}$ | $1.86 \pm 0.25$ | $1.36 \pm 0.15$ | $1.26 \pm 0.16$ | $1.54 \pm 0.32 (1.72 \pm 0.15)$ | $1.66 \pm 0.09$ | $1.67 \pm 0.17$ |
| $R_{4/2}$ | 2.14 | 2.51 | 2.68 | 2.71 | 2.67 | 2.56 |
| $R_{4/2}(0_2^+)$[a] | | | 2.01 | 2.08 | 2.11 | 2.30 |

[a]Notation $R_{4/2}(0_2^+)$ refers to the $R_{4/2}$ value in the $0_2^+$ sequence.

where $|\Phi_\kappa\rangle$ represents the set of quasiparticle (q.p.) vacuum $|0\rangle$ and 2-, 4-q.p. states for even-even nuclei. $\sigma$ specifies states with the same angular momentum $I$. To form the shell model basis in the laboratory frame, the broken rotational and axial symmetries in the deformed multi-q.p. states are necessarily recovered by exact three-dimensional angular momentum projection with an operator $\hat{P}^I_{MK}$. The two-body interaction shell model Hamiltonian is then diagonalized in the projected basis of Eq. (5).

The TPSM Hamiltonian consists of a set of separable forces,

$$\hat{H} = \hat{H}_0 - \frac{1}{2}\chi \sum_\mu \hat{Q}^\dagger_\mu \hat{Q}_\mu - G_M \hat{P}^\dagger \hat{P} - G_Q \sum_\mu \hat{P}^\dagger_\mu \hat{P}_\mu, \quad (6)$$

where $\hat{H}_0$ is the spherical single-particle Hamiltonian, which contains a proper spin-orbit force [42]. The second term is quadrupole-quadrupole ($QQ$) interaction that includes the nn, pp, and np components. The $QQ$ interaction strength $\chi$ is determined by the deformations in self-consistent relations [43]. The third term and the last term in Eq. (6) are the monopole pairing and the quadrupole pairing, respectively. In the present calculation, the strength $G_M$ has the standard form $G/A$, with $G = 20.4$ Mev for neutrons and 22.8 Mev for protons, and the quadrupole pairing strength $G_Q$ is assumed to be proportional to the monopole pairing strength, $G_Q = 0.16 G_M$, where the proportional coefficient is usually 0.12–0.18. The q.p. states are obtained from the Nilsson single-particle states through BCS transformation in a model space with three major shells for each kind of nucleon (major shells 4, 5, 6 for neutrons and 3, 4, 5 for protons in this work).

For $^{178,180,182,184}$Pt nuclei, the single-particle states are generated by the triaxially deformed Nilsson Hamitonian with the deformation parameters ($\varepsilon_2$,$\gamma$) listed in Table III. The adopted elongation deformations $\varepsilon_2$ are in consistent with that obtained by the total Routhian surface (TRS) calculations, and the $\gamma$ deformations have been chosen to reasonably reproduce the experimental $\gamma$ bands in these nuclei. Figure 7 shows the calculated yrast band and $\gamma$ band, energy as a function of spin, in comparison with the experimental data. It is demonstrated that for both the yrast bands and the $\gamma$ bands in the neutron-deficient Pt nuclei the theoretical calculations can reproduce the measured energies within the framework of the deformed shell model. The present TPSM calculations suggest that the yrast states present the collective rotation of a triaxially deformed nuclear system. This conclusion was also reached from the previous TPSM calculations which reproduce the experimental data for the light Pt isotopes with the quadrupole deformation parameters close to the ones in Table III; see Ref. [44]. Similar to TPSM, the interacting boson model (IBM) has also been used to reproduce the experimental data with the single nuclear configuration, without invoking the intruder states with distinctly different deformation; see Ref. [8]. It should be mentioned that the investigations of the structure in the light Pt nuclei have been carried out based on the assumption of shape coexistence, for example, for $^{176,178}$Pt [32,45], $^{182}$Pt [34,35], $^{184}$Pt [36], and $^{186}$Pt [35] where the $E2$ transition probabilities rather than the energies of levels were most emphasized as the evidence for shape coexistence.

The $E2$ transition probabilities have been calculated for $^{178,180,182,184}$Pt nuclei with the wave functions adopted from Fig. 7, namely, the ones to reproduce the yrast levels and the $\gamma$ band levels together. In the calculations of the $E2$ matrix elements, the standard effective charges of $0.5e$ for neutron and $1.5e$ for proton are employed. The calculated $B(E2)$

TABLE III. The elongation deformation parameter $\epsilon_2$ and the triaxial deformation parameter $\gamma$ employed in the TPSM calculation for $^{178-184}$Pt.

| | $^{178}$Pt | $^{180}$Pt | $^{182}$Pt | $^{184}$Pt |
|---|---|---|---|---|
| $\epsilon_2$ | 0.272 | 0.267 | 0.255 | 0.250 |
| $\gamma$ | 24.5 | 24.5 | 26 | 26 |

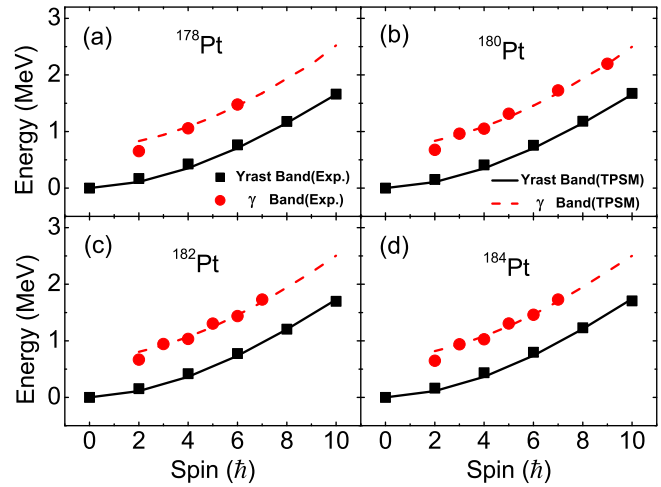


FIG. 7. Calculated yrast bands (solid line) and $\gamma$ bands (dash line), energy vs spin, for $^{178,180,182,184}$Pt by the TPSM, and the theoretical results are compared with the experimental data taken from the same references as in Table II.

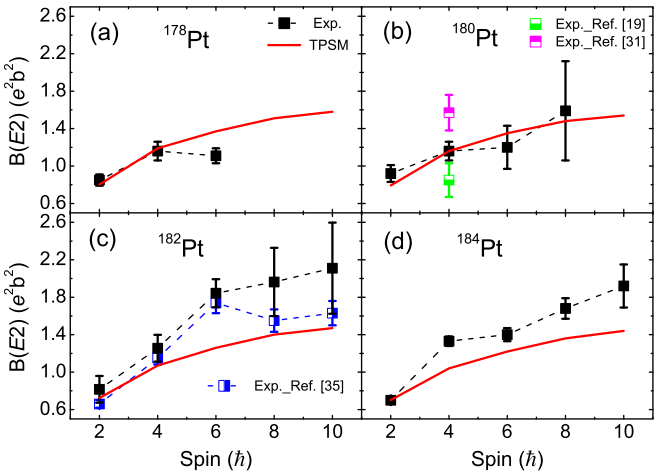


FIG. 8. Calculated $B(E2)$ values for the yrast bands in $^{178,180,182,184}$Pt by using the TPSM wave functions that reproduce the energies of the yrast states, as shown in Fig. 7. The theoretical results (solid line) are compared with the experimental data taken from the same references as in Fig. 6.

values are shown in Fig. 8 and compared to the available experimental data where the experimental $B(E2)$ values for $^{180}$Pt are extracted from the present lifetime measurements. In these light Pt isotopes, for the $E2$ transition probabilities in the ground bands, the overall spin dependence shows an increase with increasing spin. However, compared to $^{178,180}$Pt, one finds noticeably different spin dependences of $B(E2)$ values for $^{182,184}$Pt where the rapid increase with increasing spin up to $6^+$ presents. The TPSM calculations of $E2$ transition probabilities reproduce quite well the experimental data for $^{178,180}$Pt but fail in reproducing the rapidly rising behavior of experimental $B(E2)$ value for $^{182,184}$Pt. The TPSM approach considers only a single quadrupole deformation, a fixed $(\varepsilon_2,\gamma)$ value—namely, there is no mix with another distinct deformation and, hence, it cannot reproduce the rapidly rising behavior of $B(E2)$, which characterizes the shape coexistence picture. In general, the reproduction of the $B(E2)$ sharp rising behavior at low spins observed in Pt nuclei requires a mix of two distinct deformation components. For example, the $B(E2)$ experimental data for $^{182}$Pt have been reproduced by the general collective model (GCM) calculation in the framework of a mixing of bands with different quadrupole deformations [34]. A two-band mixing calculation was performed for $^{184}$Pt successfully to interpret the sharp increase of the $B(E2)$ values at low spins as the origin of shape coexistence [36]. The shape coexistence has been considered for light even-even Pt nuclei with mass smaller than $A = 188$ because the $0_2{}^+$ state lies very low in excitation energy above the ground state, typically about 500 keV [12]. However, the systematics of $B(E2)$ values at low spins do not support this criteria for the shape coexistence and, instead, show a phase transition that the sharp increase of the measured $E2$ transition probabilities from $0^+$ to $6^+$ states presents for $^{182,184}$Pt but not for $^{178,180}$Pt, as shown in Fig. 8. This sudden change for the behavior of $B(E2)$ value implies that the structure of the components in the wave function may undergo a change when going from $^{180}$Pt to $^{182}$Pt, which may cause a corresponding change in the shape coexistence picture. The present lifetime measurements of the yrast states for $^{180}$Pt have made the $B(E2)$ systematics possible for the transitional Pt region. The systematics of the experimental lifetime data and the corresponding TPSM calculations show the striking feature that a phase transition may occur at $^{180}$Pt nucleus whereafter the shape coexistence picture becomes apparent. For the $A > 186$ even-even Pt isotopes the shape coexistence would disappear because the $0_2{}^+$ states have much higher excitation energy above the ground state. However, compared to the excitation energy of the $0_2{}^+$ state, the lifetime measurements can be more essential for the identification and study of the shape coexistence in Pt nuclei with $A > 186$.

Recently, the Hartree-Fock-Bogoliubov (HFB) total energy surface calculations have been carried out for even-even $^{172-194}$Pt isotopes, and the results show the potentials have $\gamma$-softness deformation in the mass region and, particularly, the interesting feature that the energy difference between the oblate and prolate shapes is about 500 keV larger for $^{180}$Pt than for $^{182}$Pt while such an oblate-prolate energy difference is only about 100 keV larger for $^{178}$Pt than for $^{180}$Pt as well as for $^{182}$Pt than for $^{184}$Pt [13], indicating a distinguished change in the energy surface when going from $^{178,180}$Pt to $^{182,184}$Pt. Similar results have been also obtained in the Gogny-D1S interaction [46]. This feature of the energy surface change may imply that the dynamic shape fluctuation could undergo a change when going from $^{180}$Pt to $^{182}$Pt and, consequently, affect the respective shape coexistence so that a phase transition may occur when going from $^{180}$Pt, where the single prolate shape dominates the ground state, to $^{182}$Pt, where a proper mixing of oblate and prolate shapes governs the ground state. This argument may not provide a solution for the problem encountered but a possible consideration from the viewpoint of the mean field approximation. The $\gamma$ softness and the low-lying oblate minima predicted by the energy surface calculations in the framework of the mean field theory should be a reasonable request for the coexistence of the oblate ($\gamma = 60^\circ$) and prolate ($\gamma = 0^\circ$) shapes. The possible sudden change of the shape coexistence, from $^{180}$Pt to $^{182}$Pt, suggested in the systematics of the lifetime measurements is still open for a certain interpretation.

## V. CONCLUSIONS

We have measured the lifetimes of the yrast states in $^{180}$Pt from $4_1{}^+$ to $8_1{}^+$ by using the recoil distance Doppler-shift technique. A relatively slow increase in the $B(E2)$ values with increasing spins has been observed in the present work, which is different from the rapid increase of the $B(E2)$ values observed in higher-mass Pt isotopes characterizing the shape coexistence picture. The triaxial projection shell model calculations have been performed for the states of the yrast band and the $E2$ transition probabilities along the yrast band in $^{178,180,182,184}$Pt. The present calculation reproduces very well the experimental energies of the yrast states and the $B(E2)$ values for $^{180}$Pt, which indicates the nature of a deformed rotor as the TPSM calculation includes only a single quadrupole deformation. It is also demonstrated that the TPSM calculation of the $B(E2)$ values cannot reproduce the experimental data for $^{182,184}$Pt where the $B(E2)$ values increase rapidly at low

spins up to $6_1^+$ although the experimental energies of the yrast states are reproduced very well by the same TPSM calculation. The description of such fast increase in $B(E2)$ values require a consideration of the shape coexistence which has been realized, e.g., by means of the two-band mixing method. The present lifetime measurements have made the systematics of the $B(E2)$ values possible for light transitional Pt nuclei, where the feature of sharp increase of the $B(E2)$ values disappears when going from $^{182,184}$Pt to $^{178,180}$Pt. Such a sudden change of behavior of the $E2$ transition probabilities in function of spin has not been understood and the problem remains a challenge for further experimental and theoretical studies.

## ACKNOWLEDGMENTS

Valuable discussions with Q. B. Chen of Peking University are acknowledged. We are also grateful to the HI-13 tandem accelerator staff for the operation of the machine and to Q. W. Fan for his assistance during target preparation. The presentation has benefited from D. Garcia of the University of Science and Technology of China. This work is supported by the National Natural Science Foundation of China under Contracts No. 11375267, No. 11305269, No. 11175259, No. 11475072, No. 11405274, No. 11475072, No. 11575290, No. 11321064, and No. 11275068.

[1] K. Heyde and J. L. Wood, Rev. Mod. Phys. **83**, 1467 (2011).
[2] K. Heyde, P. Van Isacker, M. Waroquier, J. L. Wood, and R. A. Meyer, Phys. Rep. **102**, 291 (1983).
[3] J. L. Wood, K. Heyde, W. Nazarewicz, M. Huyse, and P. Van Duppen, Phys. Rep. **215**, 101 (1992).
[4] A. N. Andreyev *et al.*, Nature (London) **405**, 430 (2000).
[5] R. Julin, K. Helariutta, and M. Muikku, J. Phys. G: Nucl. Part. Phys. **27**, R109 (2001).
[6] K. Nomura, R. Rodríguez-Guzmán, and L. M. Robledo, Phys. Rev. C **87**, 064313 (2013).
[7] P. M. Davidson *et al.*, Nucl. Phys. A **657**, 219 (1999).
[8] E. A. McCutchan, R. F. Casten, and N. V. Zamfir, Phys. Rev. C **71**, 061301(R) (2005).
[9] E. A. McCutchan and N. V. Zamfir, Phys. Rev. C **71**, 054306 (2005).
[10] I. O. Morales, A. Frank, C. E. Vargas, and P. VanIsacker, Phys. Rev. C **78**, 024303 (2008).
[11] J. E. García-Ramos and K. Heyde, Nucl. Phys. A **825**, 39 (2009).
[12] J. E. García-Ramos, V. Hellemans, and K. Heyde, Phys. Rev. C **84**, 014331 (2011).
[13] J. E. García-Ramos, K. Heyde, L. M. Robledo, and R. Rodríguez-Guzmán, Phys. Rev. C **89**, 034313 (2014).
[14] R. Bengtsson, J. Y. Zhang, J. H. Hamilton, and L. K. Peter, J. Phys. G: Nucl. Phys. **12**, L223 (1986).
[15] R. Bengtsson, T. Bengtsson, J. Dudek, G. Leander, W. Nazarewicz, and J. Y. Zhang, Phys. Lett. B **183**, 1 (1987).
[16] M. Veskovic, M. K. Harder, K. Kumar, and W. D. Hamilton, J. Phys. G: Nucl. Phys. **13**, L155 (1987).
[17] B. Cederwall, R. Wyss, A. Johnson, J. Nyberg, B. Fant, R. Chapman, D. Clarke, F. Khazaie, J. C. Lisle, J. N. Mo, J. Simpson, and I. Thorslund, Z. Phys. A **337**, 283 (1990).
[18] J. L. Wood, *4th International Conference on Nuclei Far from Stability*, Helsingør, Denmark, CERN-81-09 (1981), p. 612.
[19] M. J. A. De Voigt, R. Kaczarowski, H. J. Riezebos, R. F. Noorman, and J. C. Bacelar, Nucl. Phys. A **507**, 472 (1990).
[20] A. Dewald, O. Möller, and P. Petkov, Prog. Part. Nucl. Phys. **67**, 786 (2012).
[21] A. Dewald, P. Sala, R. Wrzal, G. Böhm, D. Lieberz, G. Siems, R. Wirowski, K. O. Zell, A. Gelberg, and P. von Brentano, Nucl. Phys. A **545**, 822 (1992).
[22] R. Krücken, J. Res. Natl. Inst. Stand. Technol. **105**, 53 (2000).
[23] *N661_Datasheet Manual [Z]* (Physik Instrumente, 2010).
[24] *TH2817A Operation Manual [Z]* (Changzhou Tonghui Electronic Co., Ltd., 2011).
[25] A. Dewald, S. Harissopulos, and P. von Brentano, Z. Phys. A **334**, 163 (1989).
[26] G. Böhm, A. Dewald, P. Petkov, and P. von Brentano, Nucl. Instrum. Methods Phys. Res., Sect. A **329**, 248 (1993).
[27] P. Petkov, Nucl. Instrum. Methods Phys. Res., Sect. A **349**, 289 (1994).
[28] O. Möller, A. Dewald, P. Petkov, B. Saha, A. Fitzler, K. Jessen, D. Tonev, T. Klug, S. Heinze, J. Jolie, P. vonBrentano, D. Bazzacco, C. A. Ur, E. Farnea, M. Axiotis, S. Lunardi, G. deAngelis, D. R. Napoli, N. Marginean, T. Martinez, M. A. Caprio, and R. F. Casten, Phys. Rev. C **74**, 024313 (2006).
[29] H. Morinaga and T. Yamazaki, in *Beam γ-ray Spectroscopy [M]* (North Holland Publishing, Amsterdam, Netherlands, 1976).
[30] S.-C. Wu and H. Niu, Nucl. Data Sheets **100**, 483 (2003).
[31] E. Williams, C. Plettner, E. A. McCutchan, H. Levine, N. V. Zamfir, R. B. Cakirli, R. F. Casten, H. Ai, C. W. Beausang, G. Gurdal, A. Heinz, J. Qian, D. A. Meyer, N. Pietralla, and V. Werner, Phys. Rev. C **74**, 024302 (2006).
[32] G. D. Dracoulis, A. E. Stuchbery, A. P. Byrne, A. R. Poletti, S. J. Polett, J. Gerl, and R. A. Bark, J. Phys. G: Nucl. Phys. **12**, L97 (1986).
[33] C. B. Li, F. Q. Chen, X. G. Wu, C. Y. He, Y. Zheng, G. S. Li, Q. M. Chen, Z. C. Gao, Q. L. Xia, W. P. Zhou, S. P. Hu, H. W. Li, J. L. Wang, J. J. Liu, Y. H. Wu, and P. W. Luo, Phys. Rev. C **90**, 047302 (2014).
[34] K. A. Gladnishki *et al.*, Nucl. Phys. A **877**, 19 (2012).
[35] J. C. Walpe, U. Garg, S. Naguleswaran, J. Wei, W. Reviol, I. Ahmad, M. P. Carpenter, and T. L. Khoo, Phys. Rev. C **85**, 057302 (2012).
[36] U. Garg *et al.*, Phys. Lett. B **180**, 319 (1986).
[37] G. Gneuss and W. Greiner, Nucl. Phys. A **171**, 449 (1971).
[38] A. S. Davydov and G. F. Filippov, Nucl. Phys. **8**, 237 (1958).
[39] M. S. Basunia, Nucl. Data Sheets **107**, 791 (2006); E. Achterberg, O. A. Capurro, and G. V. Marti, *ibid.* **110**, 1473 (2009); B. Singh and J. C. Roediger, *ibid.* **111**, 2081 (2010); C. M. Baglin, *ibid.* **111**, 275 (2010); **99**, 1 (2003).
[40] J. A. Sheikh and K. Hara, Phys. Rev. Lett. **82**, 3968 (1999).
[41] Z.-C. Gao, Y. S. Chen, and Yang Sun, Phys. Lett. B **634**, 195 (2006).
[42] T. Bengtsson and I. Ragnarsson, Nucl. Phys. A **436**, 14 (1985).
[43] K. Hara and Y. Sun, Int. J. Mod. Phys. E **4**, 637 (1995).
[44] G. H. Bhat, J. A. Sheikh, Y. Sun, and U. Garg, Phys. Rev. C **86**, 047307 (2012).
[45] G. D. Dracoulis, Phys. Rev. C **49**, 3324 (1994).
[46] R. Rodríquez-Guzmán, P. Sarriguren, L. M. Robledo, and J. E. García-Ramos, Phys. Rev. C **81**, 024310 (2010).